3. B. L. Golden, T. R. Cech, in *The RNA World, Second Edition*, R. F. Gesteland, T. R. Cech, J. F. Atkins, Eds. (CSHL Press, Cold Spring Harbor, New York, 1999), pp. 321–349.
4. W. A. Decatur, C. Einvik, S. Johansen, V. M. Vogt, *EMBO J.* **14**, 4558 (1995).
5. C. Einvik, H. Nielsen, E. Westhof, F. Michel, S. Johansen, *RNA* **4**, 530 (1998).
6. S. Johansen, C. Einvik, H. Nielsen, *Biochimie* **84**, 905 (2002).
7. S. Johansen, V. M. Vogt, *Cell* **76**, 725 (1994).
8. C. Einvik, W. A. Decatur, T. M. Embley, V. M. Vogt, S. Johansen, *RNA* **3**, 710 (1997).
9. E. Jabri, S. Aigner, T. R. Cech, *Biochemistry* **36**, 16345 (1997).
10. A. Vader, H. Nielsen, S. Johansen, *EMBO J.* **18**, 1003 (1999).
11. W. A. Decatur, S. Johansen, V. M. Vogt, *RNA* **6**, 616 (2000).
12. Materials and Methods are available as supporting material on *Science* Online.
13. J. D. Reilly, J. C. Wallace, R. F. Melhem, D. W. Kopp, M. Edmonds, *Methods Enzymol.* **180**, 177 (1989).
14. P. Agback *et al.*, *J. Biochem. Biophys. Methods* **27**, 229 (1993).
15. N. Cougot, E. van Dijk, S. Babajko, B. Séraphin, *Trends Biochem. Sci.* **29**, 436 (2004).
16. A. B. Birgisdottir, S. Johansen, *Nucleic Acids Res.* **33**, 2042 (2005).
17. This paper is dedicated to Jan Engberg, who died of cancer on 20 December 2004. The work was supported by grants (to H.N.) from Vera and Carl Johan Michaelsens Fund, the NOVO Nordic Foundation, and the Carlsberg Foundation. We thank F. Frenzel for technical assistance, J. Kjems and B. Hove-Jensen for supplying reagents, and J. Christiansen for helpful suggestions to the manuscript. E.W. thanks the Institut Universitaire de France for support.

Supporting Online Material
www.sciencemag.org/cgi/content/full/309/5740/1584/DC1
Materials and Methods
SOM Text
Figs. S1 to S5
References and Notes

15 April 2005; accepted 29 July 2005
10.1126/science.1113645

Structural Evidence for a Two-Metal-Ion Mechanism of Group I Intron Splicing

Mary R. Stahley and Scott A. Strobel*

We report the 3.4 angstrom crystal structure of a catalytically active group I intron splicing intermediate containing the complete intron, both exons, the scissile phosphate, and all of the functional groups implicated in catalytic metal ion coordination, including the 2′-OH of the terminal guanosine. This structure suggests that, like protein phosphoryltransferases, an RNA phosphoryltransferase can use a two-metal-ion mechanism. Two Mg^{2+} ions are positioned 3.9 angstroms apart and are directly coordinated by all six of the biochemically predicted ligands. The evolutionary convergence of RNA and protein active sites on the same inorganic architecture highlights the intrinsic chemical capacity of the two-metal-ion catalytic mechanism for phosphoryl transfer.

Divalent metal ions are used in the active sites of a variety of protein phosphoryltransfer enzymes, including those required for replication, transcription, and cell signaling (*1*–*3*). Structural and biochemical studies of these proteins have shown that many, including all polymerases, use a two-metal-ion mechanism to promote catalysis (*4*, *5*). In these enzymes, a pair of divalent metals, located 3.8 to 5.0 Å apart, are used to position substrates, activate the nucleophile, and stabilize the charge on both the leaving group and the scissile phosphate (*6*–*8*).

Many RNA-based phosphoryltransferases also require direct coordination to active-site Mg^{2+} ions, including self-splicing introns, ribonuclease P, and the spliceosome when it catalyzes pre-mRNA splicing (*9*). Both chemical steps of group I intron splicing require divalent metals, and several of the ligands for these metals have been biochemically identified (Fig. 1B) (*10*–*15*). What has remained unclear are the structural details of metal-ion coordination in the RNA active site. Recent crystal structures have provided information on the fold of the group I intron and the structural basis for splice site selection (*16*–*19*); however, each of these structures included only one active-site Mg^{2+}, and all were inactive (Fig. 1B and fig. S1) (*20*). An independent model derived from biochemical analysis invokes three active-site metals and a coordination geometry for these metals different from that observed in protein enzymes (Fig. 1C) (*21*, *22*).

We have determined the crystal structure of an intron splicing intermediate that includes all metal-ion ligands and thereby retains the ability to catalyze exon ligation at a slow rate. We formed this crystallization construct by annealing a transcript comprising the majority of the *Azoarcus sp.* pre-$tRNA^{Ile}$ group I intron with two oligonucleotides, capturing the intron just before the second step of splicing (pre-2S) (Fig. 1A) (*23*). One 22-residue oligonucleotide, rcirc, represents the 3′-end of the intron and the 3′-exon. The second, a trimer (CAT), mimics the 5′-exon. The critical difference between this construct and the previously reported *Azoarcus* group I intron structure is the inclusion of the ribose at the terminal guanosine (ωG) position. The ωG O2′ has been biochemically identified as an essential ligand for a catalytic metal ion that increases the rate of splicing at least a millionfold (*24*, *25*). In order to slow the reaction sufficiently for crystallization, the complex contains a single 2′-deoxy substitution at the last nucleotide of the 5′-exon, U-1. This functional group contributes ~1000-fold to chemistry through a hydrogen bonding network that appears to be independent of metal-ion coordination (*19*, *26*, *27*). Crystals of the ribo-ωG intron in complex with the RNA binding protein U1A were obtained under conditions similar to those reported for the deoxy-ωG complex (*19*, *23*).

The crystallized RNA was able to promote exon splicing when the ribo-ωG pre-2S crystals were soaked with a radiolabeled 5′-exon substrate containing either a ribose (CAU) or a 2′-deoxyribose (CAT) at U-1 (Fig. 2A) (*28*). For this reaction to occur, the labeled substrate must have displaced the CAT cocrystallized in the intron complex. For crystals soaked with CAU or CAT, the extent of reaction after 50 hours was similar to that observed in solution under conditions designed to mimic those within the crystal (~15% and ~3% reacted, respectively) (Fig. 2, A and B). Incomplete reaction is likely to reflect the stoichiometry of the reactants and the equilibrium between the forward and reverse splicing reactions (*19*, *29*). No spliced exon product resulted from the combination of oligonucleotides used in the previous structure determination (Fig. 2A, lane 4). The crystals did not change in appearance upon addition of CAU, but diffraction was substantially reduced, likely resulting from an increase in heterogeneity of the RNA. These data demonstrate that the ribo-ωG pre-2S complex is in a catalytically accessible conformation within the crystals.

We determined the 3.4 Å structure of the ribo-ωG pre-2S group I intron complex using the experimental phases from the deoxy-ωG structure followed by refinement (supporting text) (*23*). Because the RNA in the ribo-ωG structure is primarily in the unspliced form because of the inclusion of a deoxy at U-1, the model is exclusively of the pre–second step reaction state. Although the overall architecture of the ribo-ωG pre-2S complex was essentially unchanged, the identity and position of metal ions in the active site were substantially different from those observed in the deoxy-ωG pre-2S structure (*16*).

An F_O-F_C difference map calculated before metal modeling revealed two large peaks (5σ)

Department of Molecular Biophysics and Biochemistry, Yale University, 260 Whitney Avenue, New Haven, CT 06520–8114, USA.

*To whom correspondence should be addressed. E-mail: scott.strobel@yale.edu

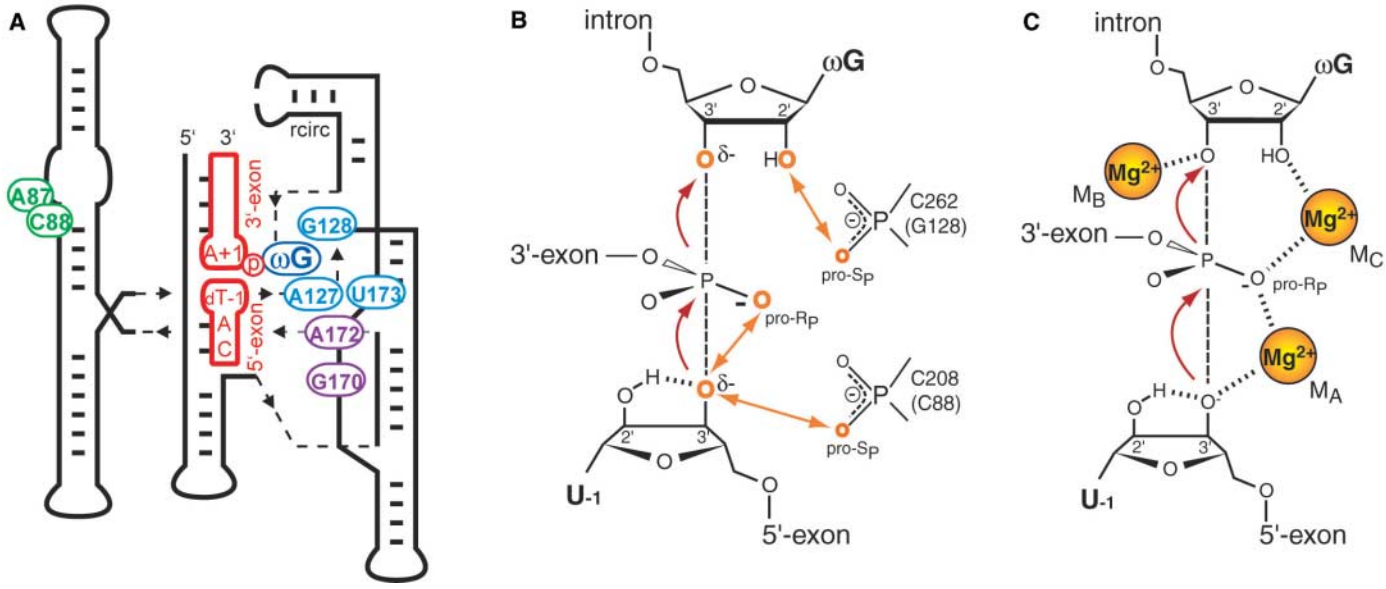

Fig. 1. The group I intron splicing reaction. (**A**) Secondary structure of the pre-2S crystallization construct. The residues discussed in the text are shown superimposed on the secondary structure. RNA connectivity is depicted with a dashed line with small arrows to show the 5′ to 3′ orientation. Exons are shown in red. The coloring of other residues corresponds to the structural element in which they are located: P4 to P6 (green), P3 to P9 (blue), and J8/7 (purple). (**B**) Summary of the biochemically defined ligands for active-site metal coordination. The six oxygens shown in orange have been implicated in metal-ion coordination on the basis of metal specificity switch experiments (*10*–*15*), including four in the substrates and two in the intron. Ligands biochemically shown to coordinate the same metal are depicted with double-ended arrows. The exon splicing reaction involving attack of the U-1 O3′ on the scissile phosphate with loss of the ωG O3′ is shown with curved arrows. (**C**) Proposed three-metal-ion mechanism based on differential Mn^{2+} affinity to sulfur/amino-substituted substrates (*21*, *22*). The four substrate ligands in (B) are coordinated to three metal ions, M_A, M_B, and M_C.

of native electron density in the active site (Fig. 3A). These peaks were assigned as Mg^{2+} ions based on the anomalous density observed for binding of a Mg^{2+} mimic at each site. Yb^{3+} bound at site M_1, and Mn^{2+} bound at site M_2 [(*30*) and supporting text]. The bond distances (all ~2.1 Å) and octahedral coordination geometry also indicate Mg^{2+} binding at both sites (Fig. 3B). The two metals have inner sphere coordination to nine oxygens, including all six of the biochemically predicted ligands (Figs. 1B and 3, B and C). In both cases, five of the metals' six possible coordination positions were satisfied by direct contacts to RNA functional groups. In each case, an additional phosphate oxygen (U173 pro-S_P oxygen for M_1 and A87 pro-S_P oxygen for M_2) appeared to make an outer sphere contact, fully satisfying the metals' octahedral coordination geometry. Density for the bridging waters was not visible at this resolution.

The two metals are well positioned to promote catalysis of the exon ligation reaction (Fig. 3B). M_1 shows direct coordination to the nucleophile (O3′ of U-1) and the scissile phosphate pro-R_P oxygen; it is equivalent to the metal observed in the deoxy-ωG pre-2S complex (*16*). Substantial changes in the identity and location of the second metal ion were observed upon inclusion of the ωG 2′-OH. A K^+ was bound near site M_2 in the deoxy-ωG structure, but it was too far away to make direct contact with the scissile phosphate (*16*). In the native ribo-ωG complex, the Mg^{2+} at M_2 was 2.5 Å closer to the scissile

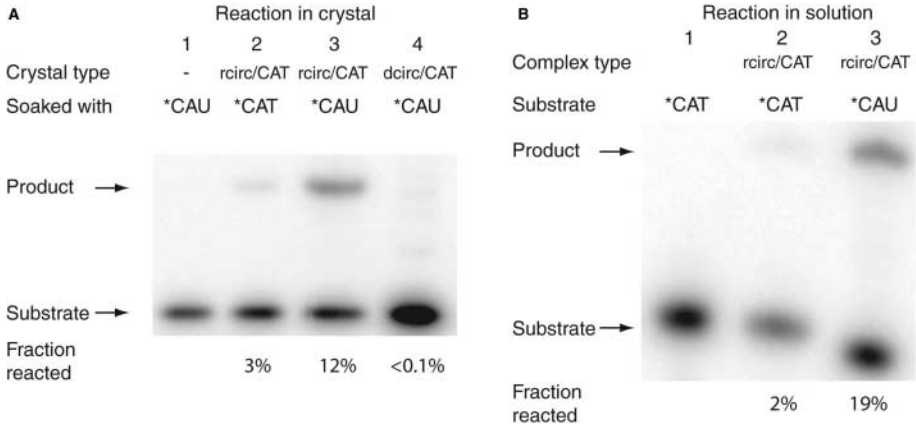

Fig. 2. Activity of the group I intron crystals. (**A**) Pre-2S crystals were soaked with an excess of ^{32}P-radiolabeled 5′-exon substrate with ribose or 2′-deoxy at U-1 (CAU or CAT, respectively). The crystals were assayed for exon ligation as described (*28*). The pair of oligonucleotides used in the original crystallization and the identity of the soaked, radiolabeled, 5′-exon substrate are indicated above the autoradiogram. (**B**) Reactivity of the complex in solution (*28*). In both panels, the fraction reacted is shown below each lane.

phosphate and the ωG O3′ leaving group. This Mg^{2+} ion makes inner sphere contacts to the scissile phosphate's nonbridging pro-R_P oxygen and both the O2′ and the O3′ leaving group of the ωG (Fig. 3B). This change in metal positioning and identity is coupled with movements of nucleotides A127 and G128 within the active site. These changes resulted in a decreased metal-to-metal distance from 5.4 Å in the deoxy-ωG structure to 3.9 Å in the ribo-ωG structure. The observed changes in metal-ion identity and coordination likely account for the more than a millionfold loss of activity observed upon 2′-deoxy ωG substitution during either step of splicing (*24*, *25*).

The coordination of M_1 and M_2 in this structure satisfies all the biochemically predicted catalytic metal-ion ligands, including four provided by the substrates and two within the intron active site (*10*–*15*) (Figs. 1B and 3B). In the three cases for which data are available, the biochemically predicted coordination of one metal by two ligands was also observed in the structure (*13*–*15*). Furthermore, the orientation of the O3′-nucleophile and scissile phosphate are ideal for inline nu-

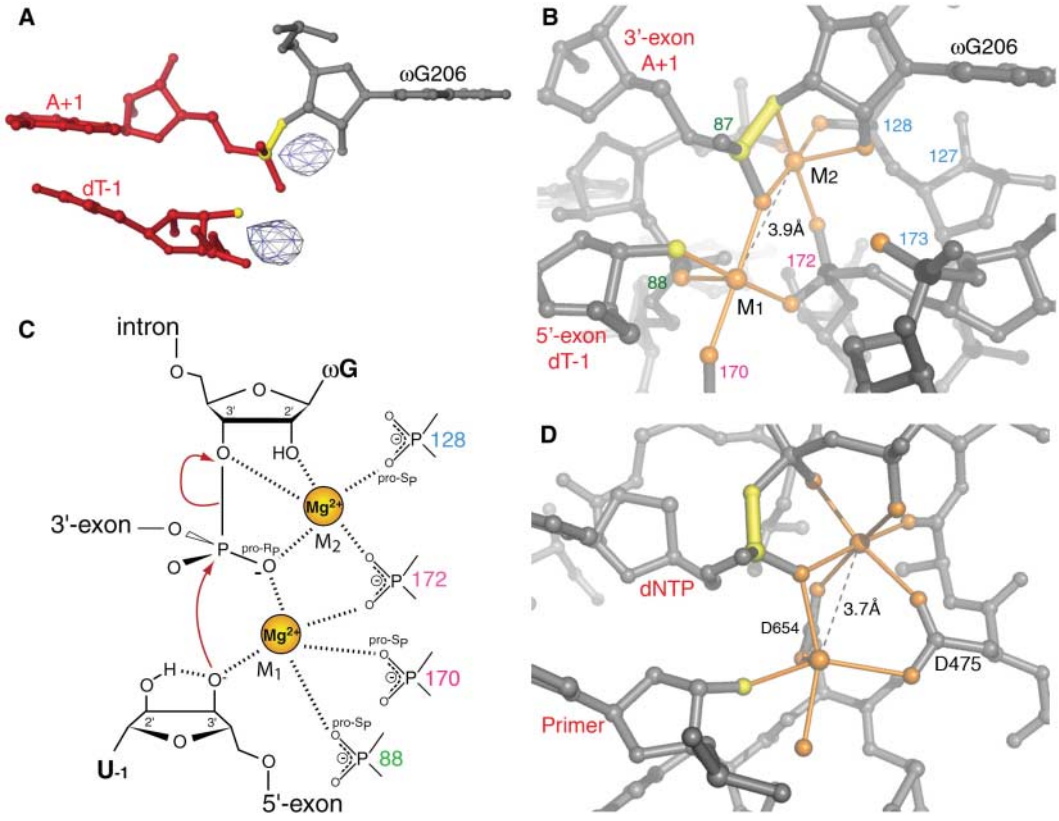

Fig. 3. A two-metal mechanism for group I intron splicing. (**A**) F_O-F_C omit map (active-site metals were not included in the model) used to assign M_1 and M_2 positions, superimposed on the refined structure. The native density (5σ) for each metal is depicted in blue. The other residues are as labeled. In (A), (B), and (D), the scissile bond, nucleophile, and leaving group are shown in yellow. (**B**) Active-site coordination to M_1 and M_2. In this and (D), the active-site Mg^{2+} ions are shown as large orange spheres, the predicted inner and outer sphere ligands are shown as small orange spheres, and the metal-to-metal distance is labeled. Orange lines indicate inner sphere coordinations. Labels for the individual nucleotides are as in Fig. 2A. All the coordinations depicted in Fig. 1B are satisfied in this structure. (**C**) Model of the group I intron transition state stabilized by a two-metal mechanism. (**D**) Two-metal active-site coordination within the T7 DNA polymerase (*1*). The incoming deoxy-nucleotide triphosphate (dNTP), the primer oligonucleotide, and active-site aspartates are labeled. The nucleophile was not present in the crystal structure but is modeled here for comparison.

cleophilic attack (the O3′–P distance is 3.2 Å, and the O3′–P–O3′ angle is 175°).

There is no evidence within this structure for a third active-site metal ion. A three-metal-ion mechanism was proposed on the basis of a difference in Mn^{2+} concentration needed to rescue different sulfur or amino substitutions of substrate functional groups. These experiments were performed on a "ground state complex" in which neither of the exons nor the critical guanosine were bound (Fig. 1C) (*21*, *22*). In this model, two different metals, M_B and M_C, are proposed to coordinate the O3′ and O2′ ligands of the ωG, respectively, resulting in different roles for the catalytic metals from those predicted by the ribo-ωG structure. Most notably, none of the metals bridge between the scissile phosphate and the leaving group in the three-metal model. Although we cannot exclude the possibility that a third metal ion is disordered in the crystal structure, the majority of the biochemical data are explained by the two metals that are observed. If a third metal is modeled near the O3′ of ωG opposite M_2, the position that is predicted in the three-metal model, the closest phosphates (ωG206 and C+2) are more than 3.5 Å away, too large a distance to make direct metal-ion coordination. Additionally, these two phosphates have never been implicated in metal-ion coordination, and it has long been established that the absence of these phosphates does not alter the activity of the reaction (*31*).

The two-metal architecture observed in this ground state structure and the bulk of the biochemical data on catalytic metal ions in group I intron splicing support a two-metal-ion mechanism for transition state stabilization, similar to that originally proposed by Steitz and Steitz based on analogy to exonuclease and phosphatase mechanisms (Fig. 3C) (*7*). M_1 (biochemically titled M_A) (*10*) activates the nucleophile, whereas M_2 (which has the dual characteristics of the biochemically titled metals M_B and M_C) (*11*, *12*) stabilizes the leaving group. Both metals bridge to the scissile phosphate, where they counterbalance the development of negative charge. In this mechanism, the active-site metal ions are symmetrical, which is consistent with a forward and reverse equilibrium for group I intron phosphoryl transfer of approximately one under standard reaction conditions (*29*). The reversible nature of the group I reaction suggests that the intron completes both steps of splicing in a similar active site. In the first step of splicing, the roles of the U-1 O3′ and G O3′ are reversed from what is observed here, in that U-1 O3′ is the leaving group and the exogenous G O3′ is the nucleophile. The roles of nucleophilic and leaving group activation for the two metals are also likely to be reversed between the two splicing reactions.

The location, coordination, and function of the active-site metals observed in this RNA active site are equivalent to a generalized two-metal-ion mechanism of catalysis employed by a wide variety of protein enzymes for the promotion of phosphoryltransfer reactions (*8*). The M_1 to M_2 distance is 3.9 Å, a hallmark of the two-metal mechanism. M_1 and M_2 share a scissile phosphate ligand and coordinate the two conjugated phosphate oxygens of A172 (Fig. 3, B and C) (*13*). Shared ligands are seen in two-metal-ion protein enzymes where both catalytic metals coordinate the scissile phosphate and bidentate carboxylates of conserved aspartate or glutamate residues (*8*, *32*). Because conjugated and shared ligands of two metals are bound less tightly than other ligands, this coordination geometry is expected to increase the Lewis acidity of the metal toward the nucleophile or leaving group and promote the reaction (*32*). The conservation of this feature between RNA and protein enzymes highlights its importance. Further, two-metal-ion mechanisms sometimes use a metal-bound water to protonate the leaving group of the reaction (*6*). M_2 has a single apical position available for a water ligand that may protonate the ωG O3′ leaving group.

There is marked similarity between this RNA active site and the active sites of RNA and DNA polymerases (Fig. 3, B and D) (*5*). The 5′-exon is analogous to the primer strand, the 3′-exon to the incoming nucleotide, and the ωG to the pyrophosphate leaving group (*33*). Both active sites contain two metal ions and coordinate those metals in a similar man-

ner. The simultaneous coordination of the scissile phosphate pro-R_P oxygen, ωG O2′, and ωG O3′ by M_2 is analogous to coordination of a single metal to the alpha, beta, and gamma phosphates of the incoming nucleotide in polymerases (*1*). RNA enzymes and protein enzymes are not evolutionarily related, so the equivalence of group I intron and polymerase active sites must be an example of convergent evolution. That macromolecular evolution arrived independently at the same solution in RNA and proteins implies an intrinsic chemical capacity of the two-metal-ion catalytic architecture for phosphoryl transfer. It is possible that this mechanism was used by the prebiotic RNA-based RNA polymerase and that it continues to be employed by other RNA splicing systems, including the spliceosome.

References and Notes

1. S. Doublie, S. Tabor, A. M. Long, C. C. Richardson, T. Ellenberger, *Nature* **391**, 251 (1998).
2. G. Zhang *et al.*, *Cell* **98**, 811 (1999).
3. R. X. Xu *et al.*, *Science* **288**, 1822 (2000).
4. N. Strater, W. N. Lipscomb, T. Klabunde, B. Krebs, *Angew. Chem. Int. Ed. Engl.* **35**, 2024 (1996).
5. L. S. Beese, T. A. Steitz, *EMBO J.* **10**, 25 (1991).
6. N. C. Horton, J. J. Perona, *Nat. Struct. Biol.* **8**, 290 (2001).
7. T. A. Steitz, J. A. Steitz, *Proc. Natl. Acad. Sci. U.S.A.* **90**, 6498 (1993).
8. N. Strater, W. N. Lipscomb, T. Klabunde, B. Krebs, *Angew. Chem. Int. Ed. Engl.* **35**, 2024 (1996).
9. M. J. Fedor, *Curr. Opin. Struct. Biol.* **12**, 289 (2002).
10. J. A. Piccirilli, J. S. Vyle, M. H. Caruthers, T. R. Cech, *Nature* **361**, 85 (1993).
11. L. B. Weinstein, B. C. Jones, R. Cosstick, T. R. Cech, *Nature* **388**, 805 (1997).
12. A. S. Sjogren, E. Pettersson, B. M. Sjoberg, R. Stromberg, *Nucleic Acids Res.* **25**, 648 (1997).
13. A. Yoshida, S. Sun, J. A. Piccirilli, *Nat. Struct. Biol.* **6**, 318 (1999).
14. A. A. Szewczak, A. B. Kosek, J. A. Piccirilli, S. A. Strobel, *Biochemistry* **41**, 2516 (2002).
15. J. L. Hougland, A. V. Kravchuk, D. Herschlag, J. A. Piccirilli, *PLoS Biol.* **3**, e277 (2005).
16. P. L. Adams, M. R. Stahley, A. B. Kosek, J. Wang, S. A. Strobel, *Nature* **430**, 45 (2004).
17. F. Guo, A. R. Gooding, T. R. Cech, *Mol. Cell* **16**, 351 (2004).
18. B. L. Golden, H. Kim, E. Chase, *Nat. Struct. Mol. Biol.* **12**, 82 (2005).
19. P. L. Adams *et al.*, *RNA* **10**, 1867 (2004).
20. Two recently reported group I intron crystal structures each contained one active-site metal ion identified by soaks with an anomalous scattering metal. The P3-P9 apo-enzyme form of the *Tetrahymena* group I intron crystal structure contained what appeared to be metal M_2. The metal was coordinated to the O2′ and O3′ of the ωG (*17*). This structure included the ωG but did not include the scissile phosphate, the 5′- or 3′-exon, or the internal guide sequence to which the exons bind. The ribozyme product form of the *Twort* intron included a single metal that appeared to be equivalent to M_1 (*18*). The metal coordinated the O3′ of U-1. This structure included the nucleophile (O3′) and the ωG but not the scissile phosphate or the 3′-exon (fig. S1).
21. S. Shan, A. Yoshida, S. Sun, J. A. Piccirilli, D. Herschlag, *Proc. Natl. Acad. Sci. U.S.A.* **96**, 12299 (1999).
22. S. Shan, A. V. Kravchuk, J. A. Piccirilli, D. Herschlag, *Biochemistry* **40**, 5161 (2001).
23. CAT and rcirc were added to a 185-nucleotide transcript before crystallization. Crystal screens were set up as described previously (*16*). Optimal crystallization conditions were 30% 2-methyl-2,4-pentanediol (MPD), 40 mM MgOAc, 40 mM KOAc, 50 mM NaCac at pH 6.7, and 0.2 mM CoHex. Crystals appeared in 2 days and reached full size in 2 weeks. Data were collected at 100 K at 1.1 Å wavelength on beamline X25 at the National Synchrotron Light Source and were processed in HKL2000 (*34*). Experimental phases were used from the deoxy-ωG structure (*16*). Refinement was performed in the program CNS (*35*), and model building was performed with the program O (*36*). Figures were made with Ribbons (*37*) and Pymol (*38*).
24. B. L. Bass, T. R. Cech, *Biochemistry* **25**, 4473 (1986).
25. S. Moran, R. Kierzek, D. H. Turner, *Biochemistry* **32**, 5247 (1993).
26. S. A. Strobel, L. Ortoleva-Donnelly, *Chem. Biol.* **6**, 153 (1999).
27. D. Herschlag, F. Eckstein, T. R. Cech, *Biochemistry* **32**, 8312 (1993).
28. Crystal activity assays were performed by washing ribo-ωG crystals in a stabilization solution of 30% MPD, 10 mM MgOAc, 10 mM KOAc, 50 mM NaCac at pH 6.8, and 0.2 mM CoHex to remove noncrystallized intron RNA. Crystals were transferred to 10 μL of this stabilization solution containing 150 μM CAU or CAT, mixed with a trace amount of ^{32}P 5′-end labeled CAU or CAT. Crystals in labeled substrate were incubated at room temperature for 2 days. The crystals were then washed extensively to remove any unbound ligation product and dissolved in a formamide denaturing buffer. The product was separated from the substrate through denaturing polyacrylamide gel electrophoresis. Ligation assays of the complex in solution were performed in the same buffer under conditions expected to mimic those found in the crystal activity assay; i.e., 1 μM transcript was mixed with 1 μM rcirc and 1 μM CAT and incubated for 30 min. To this solution was added 5 μM CAU or CAT, a trace portion of which was radiolabeled. The mixture was allowed to react for 50 hours and analyzed as described above.
29. R. Mei, D. Herschlag, *Biochemistry* **35**, 5796 (1996).
30. Crystals were soaked in 0.1 mM MnOAc or 0.5 mM $YbCl_3$ for 3 hours. Data were collected at 1.4 Å and 1.3550 Å, respectively. The Mn^{2+} soaked crystal showed a 5σ anomalous peak located over the M_2 site. The Yb^{3+} soaked crystal showed a 14σ anomalous peak located over the M_1 site. Anomalous difference maps are included as supplementary information.
31. T. R. Cech, A. J. Zaug, P. J. Grabowski, *Cell* **27**, 487 (1981).
32. G. C. Dismukes, *Chem. Rev.* **96**, 2909 (1996).
33. J. A. Doudna, J. W. Szostak, *Nature* **339**, 519 (1989).
34. Z. Otwinowski, W. Minor, *Methods Enzymol.* **276**, 307 (1997).
35. A. T. Brunger *et al.*, *Acta Crystallogr. D Biol. Crystallogr.* **54**, 905 (1998).
36. T. A. Jones, J. Y. Zou, S. W. Cowan, M. Kjeldgaard, *Acta Crystallogr. A* **47**, 110 (1991).
37. M. Carson, *J. Appl. Crystallogr.* **24**, 958 (1991).
38. DeLano Scientific (www.pymol.org).

39. We thank J. Wang for assistance with structure refinement; M. Becker and the staff at Brookhaven National Laboratory Beamline X25 for help with data collection; and T. Steitz, J. Cochrane, and L. Szewczak for critical comments on the manuscript. Supported by NSF grant no. MCB315329. Coordinates for the ribo-ωG *Azoarcus* group I intron structure are deposited in the Protein Data Bank under accession no. 1ZZN.

Supporting Online Material

www.sciencemag.org/cgi/content/full/309/5740/1587/DC1
SOM Text
Figs. S1 to S3
Tables S1 and S2
References and Notes

18 May 2005; accepted 1 August 2005
10.1126/science.1114994